Septins promote macropinosome maturation and traffic to the lysosome by facilitating membrane fusion

Lee Dolat and Elias T. Spiliotis

Department of Biology, Drexel University, Philadelphia, PA 19104

Macropinocytosis, the internalization of extracellular fluid and material by plasma membrane ruffles, is critical for antigen presentation, cell metabolism, and signaling. Macropinosomes mature through homotypic and heterotypic fusion with endosomes and ultimately merge with lysosomes. The molecular underpinnings of this clathrin-independent endocytic pathway are largely unknown. Here, we show that the filamentous septin GTPases associate preferentially with maturing macropinosomes in a phosphatidylinositol 3,5-bisphosphate–dependent manner and localize to their contact/fusion sites with macropinosomes/endosomes. Septin knockdown results in large clusters of docked macropinosomes, which persist longer and exhibit fewer fusion events. Septin depletion and overexpression down-regulates and enhances, respectively, the delivery of fluid-phase cargo to lysosomes, without affecting Rab5 and Rab7 recruitment to macropinosomes/endosomes. In vitro reconstitution assays show that fusion of macropinosomes/endosomes is abrogated by septin immunodepletion and function-blocking antibodies and is induced by recombinant septins in the absence of cytosol and polymerized actin. Thus, septins regulate fluid-phase cargo traffic to lysosomes by promoting macropinosome maturation and fusion with endosomes/lysosomes.

Introduction

Macropinocytosis is a clathrin-independent pathway of endocytosis that originates from the closure of plasma membrane ruffles into large vesicles, which internalize extracellular fluid and particles (Swanson, 2008; Kerr and Teasdale, 2009). Macropinocytosis is up-regulated by growth factors and oncogenes, which stimulate the uptake of nutrients for cell proliferation and growth (White, 2013). Many bacterial and viral pathogens invade cells by hijacking macropinocytosis, which is critical for antigen presentation (Lim and Gleeson, 2011; Mercer and Helenius, 2012; de Carvalho et al., 2015). By modulating the internalization of plasma membrane receptors and adhesion molecules, macropinocytosis is also implicated in cell signaling, adhesion, and motility (Bryant et al., 2007; Gu et al., 2011; Schmees et al., 2012).

Macropinosomes traffic to lysosomes while undergoing a process of maturation characterized by size reduction concomitant with membrane tubulation and fusion with other macropinosomes and early/late endosomes (Racoosin and Swanson, 1993; Bright et al., 2005). Macropinosome maturation is accompanied by changes in phosphoinositide and Rab GTPase content (Levin et al., 2015). Nascent macropinosomes become enriched with phosphatidylinositol 3-phosphate and Rab5 (Yoshida et al., 2009; Feliciano et al., 2011), whereas mature macropinosomes contain phosphatidylinositol 3,5-bisphosphate (PI(3,5)P2) and Rab7 (Kerr et al., 2006, 2010). Despite our knowledge of these transitions, the molecular basis and regulation of the membrane fusion events that underlie macropinosome maturation and merging with the lysosome remain unknown.

Septins are filamentous heteromeric GTPases that associate with cell membranes and the cytoskeleton (Mostowy and Cossart, 2012; Fung et al., 2014). Plasma membrane septins are essential for the maintenance of diffusion barriers and modulate exocytosis (Caudron and Barral, 2009; Bridges and Gladfelter, 2015). Much less is known about how septins function in the endomembrane system of organelles and their communication. Septin mRNAs and proteins associate with endosomes (Baust et al., 2008; Baumann et al., 2014) and are implicated in multivesicular body formation (Traikov et al., 2014). However, how septins function in endocytic membrane traffic is not known.

Results and discussion

Septins associate preferentially with maturing macropinosomes in a PI(3,5)P2-dependent manner

We previously identified a network of septin fibers in the leading lamellae of migrating MDCK epithelia (Dolat et al., 2014b). This network is interwoven with actin stress fibers but is reduced upon mild detergent extraction, indicating that a subset of

Correspondence to Elias T. Spiliotis: ets33@drexel.edu

Abbreviations used: CB, cytoskeleton buffer; LAMP1, lysosomal associated membrane protein 1; PI(3,5)P2, phosphatidylinositol 3,5-bisphosphate; PSK, penicillin, streptomycin, and kanamycin; SIM, superresolution structured-illumination microscopy; TR, Texas red.

The Rockefeller University Press $30.00
J. Cell Biol. Vol. 214 No. 5 517–527
www.jcb.org/cgi/doi/10.1083/jcb.201603030

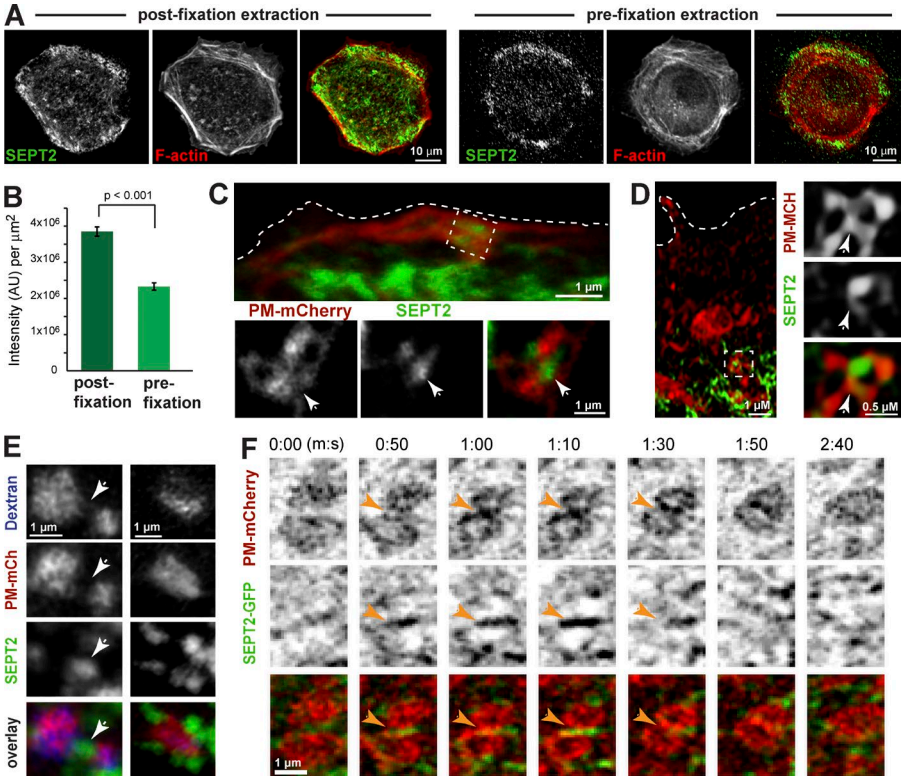

Figure 1. **Septins localize to macropinosomes and their contact/fusion sites.** (A) Confocal images of MDCKs stained for SEPT2 and F-actin with or without treatment with 0.1% Triton X-100 before fixation. (B) Bar graph shows the sum intensity (mean ± SEM) of SEPT2 per cell area (n = 15). AU, arbitrary units. (C and D) 3D-rendered confocal microscopy (C) and SIM (D) images of MDCK-PM-mCherry cells stained for endogenous SEPT2. Dashed lines outline the cell edge, and arrows point to SEPT2 at the contact sites of macropinocytic vacuoles. (E) MDCK-PM-mCherry cells were incubated with FITC-dextran and stained for SEPT2. 3D-rendered confocal images show SEPT2 at the periphery and in between (arrow) macropinosomes/endosomes. (F) MDCK-PM-mCherry cells were transfected with SEPT2-GFP and imaged live with wide-field deconvolution microscopy. Still frames show SEPT2 accumulation (arrows) at the site of fusion between two macropinosomes.

septins is membrane bound (Fig. 1, A and B). Given that membrane ruffling activity is high in cellular lamellae, we imaged the localization of septins in MDCK cells that stably express PM-mCherry (Corbett-Nelson et al., 2006), a plasmalemmal marker that marks membrane ruffles, macropinocytic vacuoles, and vesicular-tubular endosomes (Fig. S1, A and B). We stained for endogenous SEPT2 as a proxy for the lamellar network of septin fibers, which consist of SEPT2/6/7/9 (Dolat et al., 2014b). SEPT2 was largely absent from membrane ruffles but localized at the contact sites and membranes of PM-mCherry–labeled vacuoles (Fig. 1, C and D). Consistent with septin association with macropinosomes, SEPT2 localized to the periphery and in between compartments that contained PM-mCherry and dextran, a fluid-phase cargo marker that enters cells by macropinocytosis (Fig. 1 E). Time-lapse microscopy of PM-mCherry and SEPT2-GFP showed that SEPT2 accumulates at the fusion sites of macropinosomes (Fig. 1 F and Video 1); SEPT2 was present on 87 ± 12% of macropinosome contact sites (n = 11 cells).

To examine whether SEPT2 associates with early- or late-stage macropinosomes, we performed a pulse-chase experiment with fluorescent dextran. SEPT2 colocalization with dextran peaked after 5–10 min of internalization and diminished after 20–30 min (Fig. 2 A), when dextran accumulates in the lysosome (see Fig. 4 C). Given that early macropinosomes contain Rab5 whereas maturing macropinosomes become enriched with Rab7 before fusing with lysosomes (Kerr et al., 2006, 2010; Feliciano et al., 2011), we analyzed SEPT2 localization in cells that expressed Rab5- and Rab7-mCherry (Fig. S1, C–E). In peripheral lamellae, SEPT2 was present on 64 ± 4% of Rab7-positive compartments compared with 21 ± 2% of those positive for Rab5 (Fig. S1 E). SEPT2 was also present on 72 ± 4% (n = 15 cells) of peripheral vacuoles labeled with the PI(3,5)P2-binding ML1Nx2-GFP probe (Li et al., 2013), indicating that septins associate with mature PI(3,5)P2-positive macropinosomes (Fig. 2 B). Treatment of MDCK cells with YM201636, an inhibitor of the FYVE finger containing phosphoinositide kinase (PIKfyve) that converts PI3P to PI(3,5)P2 (Jefferies et al., 2008), reduced the intensity of the lamellar septin network and SEPT2 localization on dextran-containing macropinosomes (Fig. 2, C–E). Liposome flotation assays showed that SEPT2/6/7 associates preferentially with PI(3,5)P2-containing membranes (Fig. 2, F and G). In contrast to previous results with giant unilamellar vesicles (GUVs; Tanaka-Takiguchi et al., 2009), SEPT2/6/7 did not exhibit significant binding to PI(4,5)P2. Given that septin–lipid binding is sensitive to membrane curvature (Bridges et al., 2016), this discrepancy may arise from differences in the diameter of liposomes, which are 50- to 200-fold smaller than GUVs. Our results nevertheless indicate that septins associate preferentially with mature Rab7- and PI(3,5)P2-positive macropinosomes.

Septin depletion impedes the maturation and turnover of macropinosomes and reduces macropinosome fusion events

We sought to determine how septins affect macropinosome formation and dynamics by imaging PM-mCherry in live MDCK cells, which were treated with control or SEPT2 shRNAs that deplete SEPT2 but also SEPT6, 7, and 9 (Dolat et al., 2014b). In control cells, membrane ruffles gave rise to multiple macropinosomes, which fused into single vacuoles or dissipated within seconds of formation (Fig. 3 A and Video 2). In SEPT2-depleted cells, membrane ruffling and macropinosome formation were not affected. Strikingly, however, SEPT2 knock-down resulted in clusters of numerous macropinosomes (Fig. 3 A and Video 2). Clusters of three or more macropinosomes were present in fourfold more cells upon SEPT2 depletion, and the mean lifetime of nascent macropinosomes increased by 1.7-fold (Fig. 3, B and C). Notably, several macropinosomes appeared docked, with their membranes adjoining laterally (Fig. 3 E).

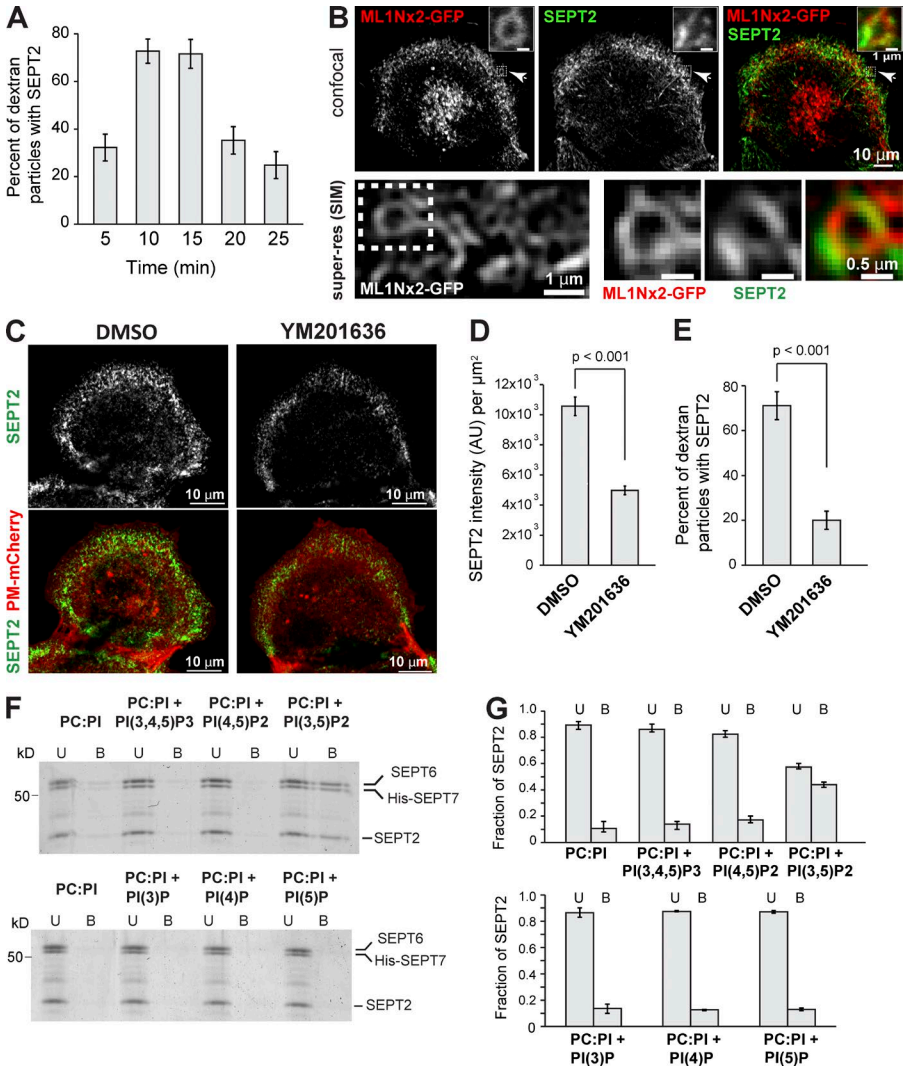

Figure 2. **Septins associate preferentially with maturing macropinosomes in a PI(3,5)P2-dependent manner.** (A) MDCKs were pulsed with TR-dextran for 5 min, chased for the indicated times, stained for SEPT2, and imaged with confocal microscopy. Bar graph shows the percentage (mean ± SEM) of dextran-containing macropinosomes/endosomes with SEPT2 (n = 12 cells). (B) Maximum-intensity projections of confocal stacks and SIM images of MDCKs transfected with ML1Nx2-GFP and stained for SEPT2. Insets show a vacuole (arrow) in higher magnification. (C) Maximum-intensity projections of confocal images of MDCK-PM-mCherry cells stained for SEPT2 after 2-h treatment with DMSO or YM201636 (800 nM). (D) Bar graph shows the sum intensity (mean ± SEM) of peripheral SEPT2 per square micrometer (n = 20 cells). AU, arbitrary units. (E) Bar graph shows the fraction (mean ± SEM) of TR-dextran puncta with SEPT2 (n = 20 cells) in MDCKs incubated with TR-dextran for 10 min after DMSO or YM201636 treatment. (F) Recombinant SEPT2/6/7 was mixed with liposomes of the indicated phosphoinositides and centrifuged on a sucrose gradient. Coomassie-stained gels show equal volumes from the top (liposome-bound SEPT2/6/7; B) and bottom (unbound SEPT2/6/7; U) fractions. (G) Bar graphs show the fraction of bound and unbound SEPT2/6/7 from three independent experiments. Error bars represent the maximum and minimum values from the three independent experiments.

In agreement with a slower macropinosome turnover, dextran uptake assays showed a significant increase in the number and size of dextran particles in SEPT2-depleted cells (Fig. 3, F and G). Notably, this increase in number and size persisted after 30 and 60 min of dextran internalization, indicating a defect in the macropinocytic traffic of dextran (Fig. 3, F and G). Similar results were obtained with a different SEPT2 shRNA (Fig. S2, A and B) and in human fibrosarcoma HT1080 cells (Fig. S2, C and D), which have intense membrane ruffling activity caused by the expression of an oncogenic mutant of N-ras (Paterson et al., 1987). Expression of an shRNA-resistant SEPT2-YFP rescued the phenotype, reversing the number and size of macropinosomes to control levels (Fig. S2 B).

Because membrane tubulation and fusion events underlie the size reduction of maturing macropinosomes, we analyzed macropinosome membrane dynamics in MDCK-PM-mCherry cells. Septin depletion did not alter the percentage (~40%) of macropinosomes that formed membrane tubules and had no effect on their detachment (Fig. 3 H and Video 3). Membrane fusion, however, was severely affected. The percentage of nascent macropinosomes that fused with another macropinosome/endosome was reduced from 74% to 25% (n = 9 cells). Moreover, the frequency of fusion events between nascent macropinosomes and tubulovesicular endosomes decreased markedly (Fig. 3 D). Thus, septins are required for the membrane fusion events underlying the shrinkage and turnover of macropinosomes.

Septins regulate fluid-phase cargo traffic and delivery to the lysosome

Given that macropinosomes transport fluid-phase cargo from the plasma membrane to the lysosome, we sought to determine whether septins affect the endocytic trafficking and lysosomal delivery of extracellular dextran. With a pulse-chase approach, MDCK cells were pulse labeled with fluorescent dextran, and its localization with respect to Rab5, Rab7, and lysosomal associated membrane protein 1 (LAMP1) was analyzed after 5, 10, and 30 min, respectively. Septin depletion did not affect dextran colocalization with Rab5 and Rab7 (Fig. S2, E–H). However, the percentage of dextran particles that colocalized with LAMP1 decreased by >60%, and this defect was rescued by shRNA-resistant SEPT2-YFP (Fig. 4, A and B). These data suggest that septins are required for the delivery of dextran to lysosomes but do not affect dextran traffic to Rab5- and Rab7-positive endosomes or the recruitment of Rab5/Rab7 to dextran-containing macropinosomes. Moreover, SEPT2 knockdown did not affect the receptor-mediated endocytosis and clathrin-dependent delivery of transferrin to Rab11 endosomes (Fig. S3, A and B).

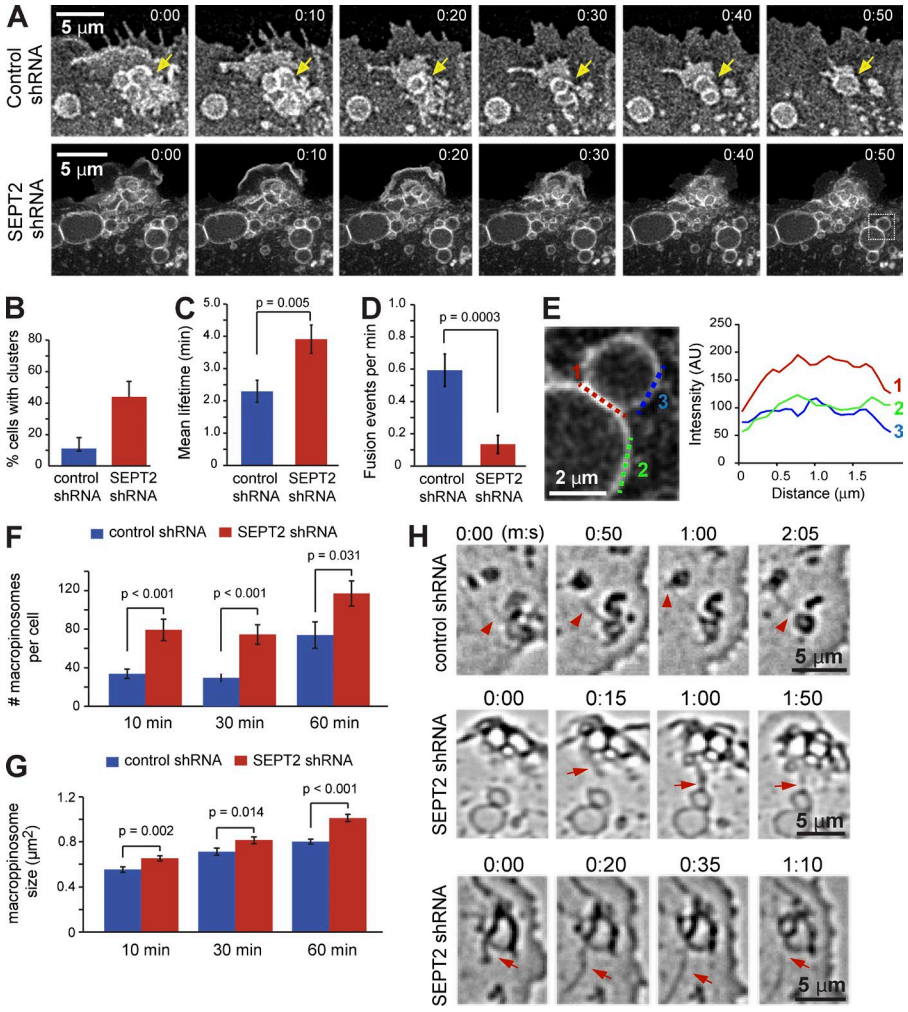

Figure 3. **Septin depletion decreases macropinocytic fusion events and hinders macropinosome maturation and turnover.** (A) Time-lapse frames from wide-field deconvolution microscopy show the dynamics of PM-mCherry–labeled macropinosomes in MDCK cells treated with control and SEPT2 shRNAs. Yellow arrow points to a cluster of macropinosomes that fuse into a single vacuole. (B) Control (n = 41) and SEPT2-depleted MDCK-PM-mCherry cells (n = 31) were imaged live every 5 s for 8 min. Bar graph shows percentage cells with a cluster of three or more macropinosomes formed from a lamellar ruffle. Error bars indicate the maximum and minimum values from three independent experiments. (C and D) Bar graphs show the lifetime (C) and fusion events (D) of nascent macropinosomes (n = 24–27). Error bars represent mean ± SEM. (E) Quantification of PM-mCherry fluorescence along the contacting (1) and noncontacting (2 and 3) segments of two macropinosomes from a SEPT2-depleted cell. AU, arbitrary units. (F and G) MDCKs were incubated with FITC-dextran for the indicated times. Bar graph-show the number of FITC-dextran–containing macropinosomes/endosomes (F) and their size (G) per cell (n = 18). Error bars represent mean ± SEM. (H) Still frames show the formation and detachment of PM-mCherry–labeled membrane tubules (arrows) in live MDCKs.

To further test whether septins regulate the lysosomal delivery of fluid-phase cargo, we analyzed kinetically the accumulation of dextran in lysosomes by quantifying dextran colocalization with LAMP1 after 5, 15, and 30 min. Between 5 and 30 min of internalization, SEPT2 depletion decreased the rate of lysosomal delivery from 2.34% to 1.02% of total dextran per minute (Fig. 4 C). Notably, the percentage of dextran colocalizing with LAMP1 in SEPT2-depleted cells did not change between 30 and 60 min of internalization (45 ± 6% vs. 50 ± 4%), which was indicative of a block in the traffic of fluid-phase cargo.

Next, we tested the effects of SEPT2 overexpression using stable MDCK cell lines that express SEPT2-YFP at low and high levels (Fig. 4 D). In the cells that express SEPT2-YFP at low levels, dextran delivery to the lysosome was similar to that of cells treated with control shRNAs (Fig. 4 E). High levels of SEPT2-YFP expression, however, increased the efficiency of dextran delivery to the lysosome (Fig. 4 E). Thus, lysosomal delivery of fluid-phase cargo is dependent on expression levels of SEPT2.

Septins promote fusion of macropinosomes with endosomes/lysosomes

To test whether septins regulate lysosomal delivery of fluid-phase cargo by directly modulating membrane fusion, we performed dual-color dextran mixing assays in live cells and in vitro using a reconstitution assay of endosomal fusion (Barysch et al., 2010).

In MDCK cells, we tested how septin knock-down affects the delivery of FITC-dextran into a cohort of endosomes/lysosomes that were preloaded with Texas red (TR)–dextran. After a 5-min pulse/15-min chase with TR-dextran, we performed 5-min pulse/15-min chase with FITC-dextran to assess its macropinocytic traffic into TR-dextran/LAMP1–positive lysosomes. Septin depletion decreased FITC-dextran entry into lysosomes with TR-dextran by 50% (Fig. 5, A and B).

Next, we performed a cell-free assay of macropinosome/endosome fusion using postnuclear extracts from two MDCK cell populations, which were labeled separately with TR- and FITC-dextran; fusion was induced with canine kidney cytosol and ATP and assayed microscopically by quantifying the fraction of endosomes with both TR- and FITC-dextran (Fig. 5, C and D). Addition of a SEPT2 function-blocking antibody or immunodepletion of SEPT2 from the cytosol abrogated fusion (Fig. 5, C–F). Surprisingly, recombinant SEPT2/6/7 and ATP induced fusion in the absence of cytosol (Fig. 5 G). Of note, addition of recombinant SEPT2/6/7 to the cytosol did not increase fusion, possibly because of saturation by cytosolic septins. Cytochalasin D, an actin-depolymerizing compound, had no effect on the endosome fusion induced by SEPT2/6/7 in the absence of cytosol and did not alter fusion in the presence of cytosol (Fig. 5, D and G). Similarly, fusion was not altered

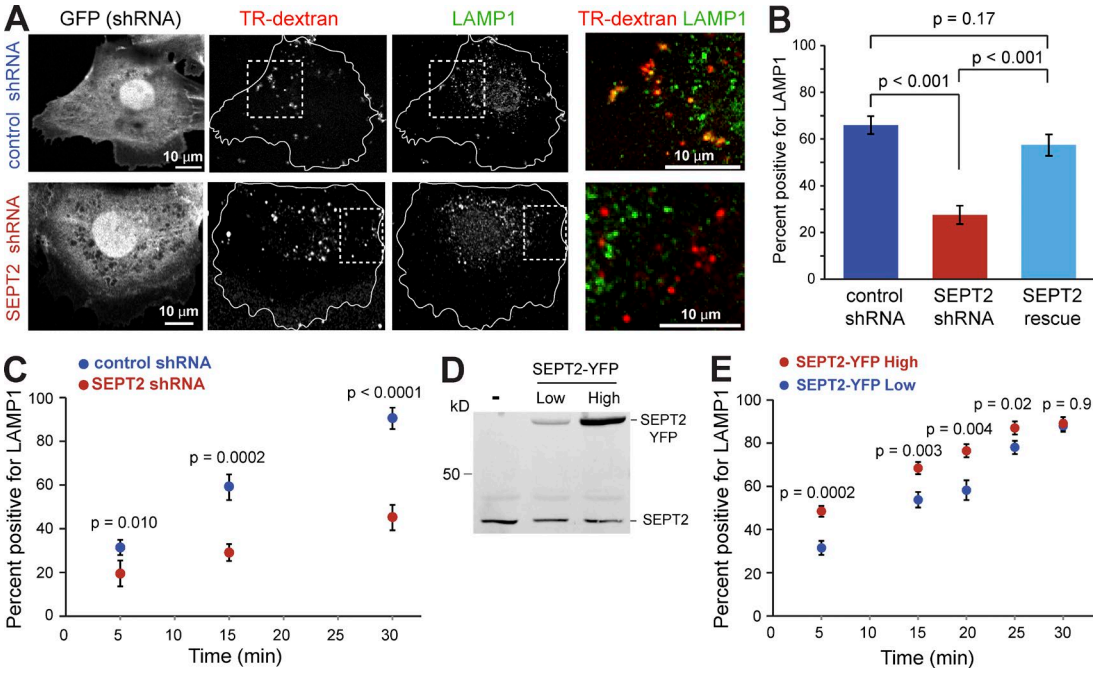

Figure 4. **Septins regulate the lysosomal delivery of fluid-phase cargo.** (A) MDCKs were transfected for 48 h with control or SEPT2 shRNAs and GFP or shRNA-resistant SEPT2-YFP (rescue). After a 5-min pulse/15-min chase with TR-dextran, cells were stained for LAMP1. Images show maximum-intensity projections of confocal image stacks. (B) Bar graph shows percentage (mean ± SEM) of TR-dextran particles that colocalize with LAMP1 (n = 20 cells). (C) Plot shows percentage (mean ± SEM) of TR-dextran with LAMP1 in control and SEPT2-depleted MDCKs (n = 15), which were pulsed with TR-dextran for 5 min and chased for the indicated times. (D) Lysates from MDCKs that stably express SEPT2-YFP at low and high levels were analyzed by SDS-PAGE and blotted for SEPT2. (E) Plot shows percentage (mean ± SEM) of TR-dextran with LAMP1 in MDCK cells (n = 14) that express SEPT2-YFP at low and high levels. Cells were pulsed with TR-dextran for 5 min and chased for the indicated times.

by the microtubule depolymerizing drug nocodazole. Thus, septins can directly induce membrane fusion independently of F-actin and microtubules.

Collectively, our results show that septins promote the membrane fusion events that underlie the maturation of macropinosomes and the delivery of fluid-phase cargo to lysosomes. This is the first evidence for a direct role of septins in clathrin-independent endocytosis and the fusion of endomembranes. In the context of exocytosis, septins interact with SNARE proteins and the exocyst complex (Hsu et al., 1998; Beites et al., 1999; Taniguchi et al., 2007; Ito et al., 2009). The SNARE and vesicle tethering complexes that mediate the fusion events of the macropinocytic pathway are largely unknown. The exocyst Sec6/8 complex localizes to the endosomes of MDCKs (Oztan et al., 2007), but septins did not colocalize with Sec6/8 or Exo70 at the contact sites of macropinosomes/endosomes (Fig. S3, C–E). Septin knock-down also did not affect the localization of Vps39 (Fig. S3, F and G), a component of the homotypic fusion and vacuole protein sorting vesicle-tethering complex (Balderhaar and Ungermann, 2013). Because septin depletion dramatically increases the fraction of docked macropinosomes/endosomes (Fig. 2), septins appear to play a distinct role in membrane fusion without affecting membrane tethering and/or docking. Notably, this septin role is coupled to PI(3,5)P2, a low-abundance phosphoinositide that is specifically involved in the fusion of mature macropinosomes/endosomes with lysosomes (Kerr et al., 2006; McCartney et al., 2014). Thus, similar to the evolutionarily related Rab GTPases, septin GTPases function as phosphoinositide effectors that catalyze SNARE-mediated fusion. Future studies will determine whether this function involves the stabilization of specific SNARE complexes and the induction or sensing of membrane curvature, which promotes lipid mixing (Martens and McMahon, 2008).

Oncogenic proteins of the Ras family of GTPases have long been known to up-regulate membrane ruffling and macropinocytosis, which in turn increases nutrient uptake to support the metabolic needs of growing cancers (White, 2013; Kimmelman, 2015). Moreover, lysosomal delivery of fluid-phase cargo (e.g., amino acids) is critical for the activation of signaling pathways that regulate cell growth and division (Commisso et al., 2013; Settembre et al., 2013). Septins are overexpressed in many cancers, but their functions in cancer are poorly understood (Connolly et al., 2011; Dolat et al., 2014a). Because SEPT2 alone does not induce fusion in vitro (Fig. 5 G) and SEPT2-YFP overexpression does not alter the expression levels of SEPT6/7 (not depicted), we posit that overexpression of a single septin (e.g., SEPT2) may promote the formation of membrane-bound SEPT2/6/7 polymers, which could functionally support the elevated macropinocytic activity of cancer cells. Future studies may explore how this novel function of septins might be therapeutically targetable.

Materials and methods

Plasmids

Mouse SEPT2 was inserted into N1-YFP (Spiliotis et al., 2005). Mouse SEPT2 was inserted into N1-GFP (Bowen et al., 2011). PM-mCherry was constructed by inserting the membrane-binding domain of lyn kinase in pcDNA 3.1-mCherry (Benjamin et al., 2010). Human Rab5A was inserted into C1-GFP using the HindIII and SalI restriction sites,

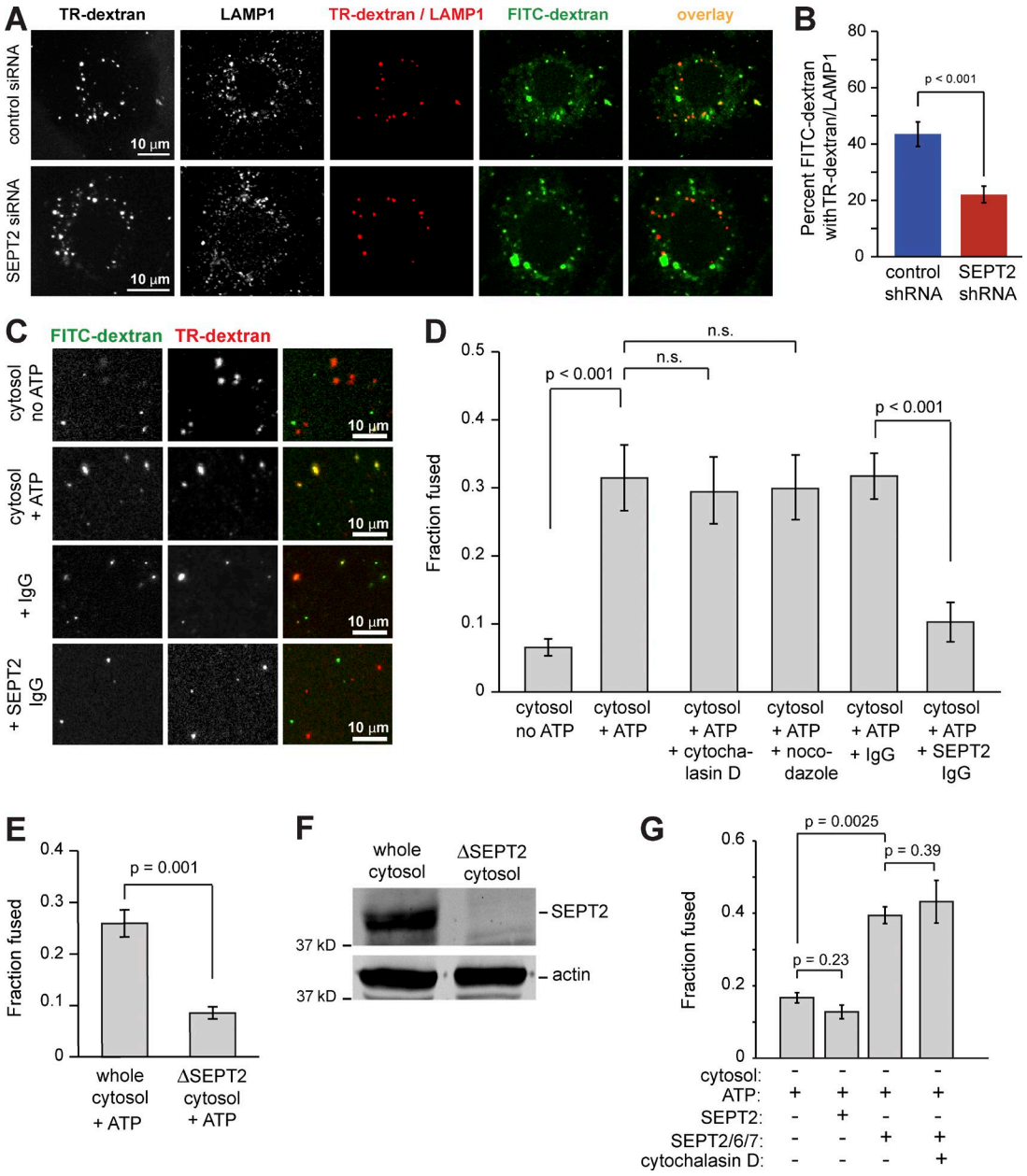

Figure 5. **Septins are required for fusion of macropinosomes/endosomes with lysosomes and promote fusion directly in an in vitro reconstitution assay.** (A) MDCKs were treated with control or SEPT2 siRNA, and two rounds of 5-min pulse/15-min chase were performed with TR- and FITC-dextran, successively. Cells were stained with anti-LAMP1 and imaged with confocal microscopy. Images show maximum-intensity projections of TR-dextran and LAMP1 and their areas of overlap (pseudo-colored in red masks), as well as FITC-dextran (green) and its overlay with the pseudo TR-dextran/LAMP1 channel. (B) Bar graph shows percentage TR-dextran/LAMP1 that contains FITC-dextran (n = 18 cells). (C and D) MDCKs were separately incubated with TR- or FITC-labeled dextran for 5 min, and postnuclear supernatants were mixed with canine kidney cytosol without or with ATP (3.3 mM) plus cytochalasin D (10 µM), nocodazole (10 µM), and control or anti-SEPT2 IgG. Images (C) show dextran-containing macropinosomes/endosomes after incubation in the indicated conditions. Bar graph (D) shows the fraction (mean ± SEM) of fused macropinosomes/endosomes with both TR- and FITC-labeled dextran (n = 15 images). n.s., not significant. (E) Bar graph shows the fraction (mean ± SEM) of fused endosomes after incubation of PNS with ATP and whole or SEPT2 immunodepleted (ΔSEPT2) cytosol (n = 15). (F) Gel shows equal volumes of whole and ΔSEPT2 cytosol blotted for SEPT2 and actin. (G) Bar graphs show the fraction (mean ± SEM) of fused endosomes after incubation of postnuclear supernatants with ATP and SEPT2 or SEPT2/6/7 (2.5 µM) in the presence/absence of 10 µM cytochalasin D (n = 15).

and human Rab7A was inserted into C1-GFP using the Xho1 and KpnI restriction sites. Human Rab5B-mCherry and human Rab7A-mCherry were purchased from Addgene. Mouse vps39 was inserted into C1-GFP (Poupon et al., 2003) and was a gift from V. Faundez (Emory University, Atlanta, GA).The tandem PI(3,5)P2-binding domains of the transient receptor potential mucolipin (TRPML1) channel was inserted into C3-GFP (Li et al., 2013) and was a gift from H. Xu (University of Michigan, Ann Arbor, MI). Rat SEPT7v2 and human SEPT6v3 were inserted into the pET-28a(+) vector, which expresses in tandem His-SEPT7 and an untagged SEPT6 (Bai et al., 2013). Mouse SEPT2 was inserted into pET-28a(+) and pET-15b, which express, respectively, a His-tagged SEPT2 and an untagged SEPT2 (Bai et al., 2013).

For experiments using shRNAs, the nontargeting control (5′-TGAGTTCACACTAATGGTGGTCG-3′) was inserted in pG-SUPER-

GFP (Bowen et al., 2011) and pSUPER-mCherry (Dolat et al., 2014b). To target canine SEPT2, the shRNA #1 (5′-CCTTAGACGTCGCAT TCATGAAA-3′) was inserted in pSUPER-mCherry (Dolat et al., 2014b) and SEPT2 shRNA #2 (5′-GCAACTACAAGCCCGAAG AATAA-3′) was inserted in pG-SUPER-GFP. Human SEPT2 was targeted using the SEPT2 shRNA 5′-AAGGTGAATATTGTGCCT GTC-3′, which was inserted in pG-SUPER-GFP (Bowen et al., 2011). For siRNA experiments (Fig. 5), the SEPT2 siRNA oligonucleotide 5′-AAGGUGAAUAUUGUGCCUGUC-3′ and control GFP siRNA oligonucleotide 5′-GGCUACGUCCAGGAGCGCACC-3′ were purchased from GE Healthcare. For the rescue experiments, the canine shRNA #2 was inserted in pGFP-V-RS (OriGene) using the BamHI and HindIII restriction sites to generate pGFP-V-RS-SEPT2-shRNA. Mouse SEPT2-YFP was PCR amplified from SEPT2-N1-YFP using the primers 5′-CAGAGATCTATGTCTAAGCAACAACC-3′ and 5′-CAGACGCGTTTACTTGTACAGCTCG-3′ and inserted in the pGFP-V-RS-SEPT2 shRNA plasmid using the BglII and MluI restriction sites.

Tissue culture and transfections

MDCK II/G cells and the stable cell lines MDCK-SEPT2-YFP (CMV promoter; N1-YFP; Spiliotis et al., 2005) and MDCK-PM-mCherry (CMV promoter; pcDNA3.1; Benjamin et al., 2010) were cultured in low-glucose DMEM with 1 g/l $NaHCO_3$, 10% FBS (Cell Generation), and 1% penicillin, streptomycin, and kanamycin (PSK) at 37°C with 5% CO_2. HT1080 cells (CCL-121) were purchased from ATCC and cultured in high-glucose DMEM with 1 g/l $NaHCO_3$, 10% FBS (Cell Generation), and 1% PSK at 37°C with 5% CO_2. Cells were plated on no. 1.5 glass coverslips (VWR International), which were precoated with 10 µg/ml type I collagen (PurCol; Advanced BioMatrix) in 0.1% acetic acid for 5 min, dried, and rinsed twice with medium before cell plating. Cells were transfected with 1.5 µg plasmid or cotransfected with 1.0 µg of one plasmid and 1.5 µg of the second plasmid using Lipofectamine 2000 (Invitrogen).

Dextran uptake and pulse-chase assays

Cells were cultured in low-serum medium (0.5% FBS) overnight and switched to medium with 10% FBS to stimulate macropinocytosis for the duration of incubations and pulse-chase treatments with fluorescent dextran. Pulse-chase experiments were performed by incubating cells with medium containing 10% FBS and 0.2 mg/ml FITC-, TR-, or Alexa Fluor 647–conjugated dextran (10,000 molecular weight; Thermo Fisher Scientific) for 5 min, washing three times, and incubating cells in dextran-free medium for the indicated times. In Fig. 2 E, cells were incubated with 800 nM YM201636 (Selleck Chemicals) or vehicle control (DMSO) for 2 h in low-serum medium and then stimulated with medium containing 10% FBS and 0.2 mg/ml TR-dextran with YM201636 or DMSO for 10 min.

Transferrin uptake assays

MDCK cells were transfected with mCherry-expressing control or SEPT2 shRNA for 48 h, cultured in low-serum medium (0.5% FBS) for 1 h at 37°C, cooled on ice for 5 min, incubated with 10 µg/ml Transferrin-488 (Thermo Fisher Scientific) in ice-cold low-serum medium for 15 min on ice, washed three times with ice-cold medium, and incubated with medium containing 10% FBS at 37°C for 5, 7.5, and 10 min. Cells were subsequently washed twice with PBS and fixed with 4% PFA.

Immunofluorescence microscopy

Cells were fixed with warm (37°C) 2% PFA in PBS and simultaneously permeabilized and blocked with 2% BSA (Sigma-Aldrich) and 0.1% saponin (EMD Millipore) for 30 min. In Fig. 1 A, cells were extracted before fixation by incubating for 30 s with warm (37°C) cytoskeleton buffer (CB) containing 10 mM MES, pH 6.1, 138 mM KCl, 3 mM $MgCl_2$, 2 mM EGTA, 320 mM sucrose, and 0.1% Triton X-100. Cells were subsequently rinsed twice with CB and fixed with 2% PFA in CB.

Rabbit antibodies against SEPT2 (N5N; a gift from M. Kinoshita, Nagoya University, Nagoya, Japan), Rab5 (Stressgen Biotechnologies), and Rab11A (Proteintech) and mouse antibodies against Rab7A (Abcam), LAMP1 (H4A3; Developmental Studies Hybridoma Bank, University of Iowa), Sec6 (Exoc3; 10C2), Sec8 (Exoc4; 9H5), Exo70 (Exoc7; 13F3; gifts from C. Yeaman, University of Iowa, Iowa City, IA), were diluted in PBS containing 2% BSA and 0.1% saponin. Secondary donkey Alexa Fluor 488–, 594–, or 647–conjugated F(ab′) to mouse or rabbit IgG (Jackson ImmunoResearch Laboratories, Inc.) was diluted in PBS containing 2% BSA and 0.1% saponin. Cells were stained for F-actin using phalloidin conjugated to Alexa Fluor 555 (ActiStain; Cytoskeleton, Inc.). Coverslips were mounted on slides using Vectashield (Vector Laboratories).

Slides were imaged using a confocal laser-scanning microscope (FluoView 1000; Olympus) equipped with three Hamamatsu R7862 photomultiplier tubes (PTMs) and multiline argon ion (458, 488, and 515 nm), helium-neon (543 nm), and diode 401- and 635-nm lasers. Images were acquired using 60×/1.42-NA oil objective and FV10-ASW 02.01 software. Superresolution structured-illumination microscopy (SIM) was performed using DeltaVision OMX V4 (GE Healthcare) with an Olympus 60×/1.42-NA objective and immersion oil with a refractive index of 1.514. Images were acquired using a 0.125 µM z-step, sCMOS pco.edge camera (custom version) and reconstructed with softWoRx software (Applied Precision Ltd.). 3D rendering of confocal stacks was performed in Volocity software (PerkinElmer).

Time-lapse imaging

All time-lapse microscopy experiments were performed at 37°C using DMEM without phenol red, supplemented with 10% FBS, 1% PSK, and 20 mM Hepes. In Figs. 1 and 3 A, PM-mCherry dynamics were imaged with 3D deconvolution wide-field microscopy using an inverted microscope (DeltaVision OMX v4; GE Healthcare) equipped with a motorized stage, stage-top incubator with temperature controller, and three pco.edge sCMOS cameras (custom version). 3D stacks (1–2 µm; 0.125-µm slices) were acquired every 10–20 s using a 60×/1.42-NA objective lens (Olympus) and were deconvolved in softWoRx 6.1.1 software. In Fig. 3 (B–D and H), macropinosome dynamics were imaged using an inverted microscope (IX81; Olympus) equipped with a motorized stage (ProScanII; Prior), an OrcaR2 charge coupled device camera (Hamamatsu Photonics), a custom-built stage-top chamber and temperature controller (Air-Therm ATX; World Precision Instruments), and Slidebook 6.0 software. Fluorescent images were acquired every 5 s for 8 min with a Plan-Apochromat 60×/1.40-NA objective. Time-lapse videos were rendered in Photoshop (Adobe Systems).

Protein expression and purification

Recombinant SEPT2/6/7 was expressed by cotransforming *Escherichia coli* BL21(DE3) cells with a kanamycin-resistant, bicistronic pET-28a(+) that expresses His-SEPT7 and SEPT6 and an ampicillin-resistant pET-15b(+) plasmid that expresses an untagged SEPT2. Recombinant SEPT2 was expressed by transforming *E. coli* BL21(DE3) cells with a kanamycin-resistant pET-28a(+) plasmid that expresses His-SEPT2. Bacterial cultures were grown to 0.6 OD and induced with 0.5 mM isopropyl β-D-1-thiogalactopyranoside for 16 h at 18°C. Cultures were centrifuged (4,000 *g*) for 10 min at 4°C and lysed in buffer containing 50 mM Tris, pH 7.5, 150 mM NaCl, 1 mM PMSF, 1 mM DTT, 10 mM imidazole, and 10% glycerol using a French pressure cell at 1,280 psi. Cell lysates were centrifuged (14,000 *g*) for 30 min at 4°C and passed through a 0.45-µm filter before being applied to a gravity flow column

with Ni-NTA beads. The columns were washed with buffer containing 50 mM Tris, pH 8.0, 300 mM NaCl, 1 mM DTT, 20 mM imidazole, and 10% glycerol, and proteins were eluted using buffer containing 50 mM Tris, pH 8.0, 150 mM NaCl, 10% glycerol, and 250 mM imidazole. Protein preparations were dialyzed overnight in dialysis buffer (50 mM Tris, pH 8.0, 150 mM NaCl, 1 mM DTT, and 10% glycerol).

Liposome flotation assays

All lipids were purchased from Avanti Polar Lipids except PI(4,5)P2 diC8 (Echelon Biosciences; p-4508). L-α-Phosphatidylcholine (840051) and L-α-phosphatidylinositol (840042) were diluted in chloroform. PI(3,4,5)P3 (850156), PI(3,5)P2 (850154), PI(3)P (850150), PI(4)P (850151), and PI(5)P (850152) were diluted in a solution made of chloroform, methanol, and water (20:9:1). PI(4,5)P2 was diluted in water. To generate small unilamellar vesicles, lipids were mixed to a final concentration of 75%mol L-α-phosphatidylcholine, 20%mol L-α-phosphatidylinositol, and 5%mol of each phosphoinositide. Lipid mixtures were dried completely under a nitrogen stream, rehydrated in liposome buffer (50 mM Hepes, pH 7.2, and 50 mM KCl) for 30 min at 25°C, frozen and thawed five times, and passed through a mini-extruder (Avanti Polar Lipids, Inc.) using a 0.1-µm pore filter at least 12 times to isolate small unilamellar liposomes. Liposomes were stored at 4°C and used within 1–2 d.

To test for septin binding, liposomes (0.5 mM) were mixed with 0.5 µM recombinant SEPT2/6/7 in 50 µl liposome buffer containing 1 mM $MgCl_2$ and incubated with rotation at 25°C for 1 h. Reactions were mixed with 100 µl liposome buffer with sucrose (75%) and placed at the bottom of a polycarbonate tube (Beckman Coulter). Liposome buffer (200 µl) with 25% sucrose was gently overlaid, and on top of that layer, 50 µl of liposome buffer was gently placed. Samples were centrifuged (220,000 *g*) in a SW60 Ti rotor (Beckman Coulter) for 1 h at 20°C. Equal volumes of the top and bottom fractions were collected with a thin pipette tip, run on a 10% SDS-PAGE gel, and stained with Coomassie brilliant blue. Gels were scanned using the Odyssey imaging system (LI-COR Biosciences). The protein gels in Fig. 2 F are representative of three independent experiments, and error bars in Fig. 2 G correspond to minimum and maximum values.

In vitro fusion assay

Reconstitution of endosome fusion was performed in a cell-free fluorescence-based assay as previously described (Barysch et al., 2010). MDCK cells were cultured on 15-cm plates to 80% confluence, trypsinized, and centrifuged (300 *g*) for 5 min. Cells were resuspended in cold PBS containing 5 mg/ml BSA (PBS-BSA) and centrifuged (250 *g*) for 5 min at 4°C. The cell pellet was resuspended in cold internalization buffer (0.2 mg/ml glucose in OPTI-MEM) and centrifuged (250 *g*) for 5 min at 4°C. The supernatant was discarded, and the pellets were incubated at 37°C for 5 min before resuspending in warm internalization buffer with either FITC- or TR-dextran (0.5 mg/ml) and incubating for an additional 5 min at 37°C. Cells were transferred to ice and washed three times with cold PBS-BSA and once with homogenization buffer (250 mM sucrose and 3 mM imidazole, pH 7.4) with centrifuging (250 *g*) for 5 min at 4°C in between washes. The cell pellet was resuspended in 1 ml homogenization buffer containing protease inhibitors (EMD Millipore), passed through a ball-bearing homogenizer 20 times, and centrifuged (1,200 *g*) for 15 min at 4°C. The postnuclear supernatant was recovered, and protein concentration was determined using a Bradford assay (Thermo Fisher Scientific). Small aliquots of the postnuclear supernatants were flash-frozen in liquid nitrogen and stored at −80°C. Canine kidney cytosol (gift from J. Nelson, Stanford University, Stanford, CA) was isolated as previously described (Davis et al., 1974). Canine kidney cortex was washed in cold PBS, cut into 1-cm cubes, and homogenized using a Waring blender in PBS containing 250 mM sucrose. The homogenate was filtered and centrifuged (100,000 *g*) to remove cell membranes, and aliquots of the supernatant were drop flash-frozen in liquid nitrogen and stored at −80°C.

Fusion reactions were assembled by mixing 5 µg of canine kidney cytosol with 0.1 µg of postnuclear extracts and FITC- and TR-dextran–labeled macropinosomes/endosomes in homogenization buffer (50 µl) with protease inhibitors and with or without 3.3 mM ATP. All reactions were incubated at 37°C for 45 min. To inhibit SEPT2 function, the cytosol was preincubated in homogenization buffer containing 0.5 mg/ml rabbit anti-SEPT2 (N5N) or rabbit IgG (Sigma-Aldrich) for 1 h at 4°C. To depolymerize actin or microtubules, reactions were incubated with 10 µM cytochalasin D (Sigma-Aldrich) and 10 µM nocodazole (Sigma-Aldrich), respectively. SEPT2 was immunodepleted from the cytosol as previously described (Pagano et al., 2004). Cytosol was diluted to 1 mg/ml in buffer containing 20 mM Hepes, pH 7.2, 90 mM potassium acetate, and 2 mM magnesium acetate with protease inhibitors and incubated with 5 µg rabbit anti-SEPT2 or rabbit IgG overnight with rotation at 4°C. Protein A beads (Thermo Fisher Scientific) were blocked with 2% BSA overnight, washed five times with homogenization buffer, and added to the cytosol for 3 h at 4°C. Samples were centrifuged (1,000 rpm) for 5 min at 4°C, and the supernatant was collected. SEPT2 protein levels in the cytosol samples were assessed by Western blot. Fusion reactions containing recombinant septins were assembled by mixing recombinant SEPT2 (2.5 µM) or the recombinant SEPT2/6/7 complex (2.5 µM) with 0.1 µg postnuclear extracts and FITC- and TR-dextran–labeled macropinosomes/endosomes in homogenization buffer (50 µl) with protease inhibitors, 3.3 mM ATP, and 10 µM cytochalasin D or DMSO.

To assess fusion microscopically, reactions (30 µl) were floated into chambers created by immobilizing a glass coverslip on a slide with two strips of double-sided tape; before mounting, coverslips were cleaned with 70% ethanol and flame-dried. Chambers were washed with homogenization buffer before adding each reaction mix and sealing with vacuum grease. Slides were centrifuged (300 *g*) upside-down for 10 min at 25°C using a swing-bucket rotor with microtiter adapters. Samples were imaged using an inverted AxioObserver Z1 wide-field microscope (ZEISS) equipped with an Orca-R2 digital charge coupled device camera (Hamamatsu Photonics), X-cite 120 metal halide lamp, and motorized z-drive. Images were acquired using a 63×/1.4-NA objective and Slidebook 6.0 software (Intelligent Imaging Innovations).

Western blots

Cells were lysed in buffer containing 50 mM Hepes, pH 7.4, 100 mM NaCl, 0.5% Triton X-100, 1 mM $MgCl_2$, 1 mM PMSF, and protease inhibitors. Samples were centrifuged at 8,000 rpm for 10 min at 4°C, and the supernatants were collected. Equal volumes were resolved with a 10% SDS-PAGE gel and transferred to a nitrocellulose membrane at 100V for 1 h at 4°C. Membranes were blocked with 5% dried milk (wt/vol) in PBS containing 0.1% Tween-20. A rabbit antibody against SEPT2 (1:5,000; Sigma-Aldrich) and a secondary anti-rabbit antibody (LI-COR Biosciences) conjugated to infrared dye was diluted in PBS containing 2% BSA, 0.1% Tween-20, and 0.025% sodium azide and sequentially incubated on the membrane before scanning with the Odyssey imaging system (LI-COR Biosciences).

In Fig. 5, equal volumes of canine kidney cytosol samples were resolved on a 10% SDS-PAGE gel and transferred to a nitrocellulose membrane. Membranes were blocked in 5% dried milk (wt/vol) in PBS containing 0.1% Tween-20. Rabbit antibody against SEPT2 (1:5,000; Sigma-Aldrich), mouse anti-actin (1:5,000; Sigma-Aldrich), and anti-rabbit or -mouse secondary antibodies (LI-COR Biosciences) conjugated to infrared dyes were diluted in PBS containing 2% BSA, 0.1% Tween-20, and 0.025% sodium azide and sequentially incubated on each membrane before scanning with the Odyssey imaging system (LI-COR Biosciences).

Image analysis and quantifications

Image analysis was performed with Slidebook 6.0 unless otherwise noted. In Figs. 1 B and 2 D, the peripheral lamellar regions of cells were masked by segmentation of F-actin or PM-mCherry fluorescence, respectively, and within these regions, the sum of SEPT2 fluorescence intensity per square micrometer was quantified in each cell. In Fig. S2 C, cell areas were masked based on the GFP (shRNA) fluorescence, and the sum of SEPT2 fluorescence per square micrometer was quantified in each cell. In Fig. 2, the percentage of dextran particles (0.5–5 μm^3) with SEPT2 was calculated by creating dextran and SEPT2 masks using fluorescence intensity segmentations. SEPT2 and dextran masks were subtracted to create a new artificial channel with masks that corresponded to all dextran fluorescence that overlapped with SEPT2. The particles of this overlay channel were automatically counted, and their number was divided by the total number of dextran particles to derive the percentage of dextran that colocalizes with SEPT2. The same approach was used to derive the percentage of dextran particles (0.5–5 μm^3) with Rab5, Rab7, Vps39-GFP, and LAMP1 (Figs. 4, S2, and S3); LAMP1 background fluorescence was subtracted by Gaussian smoothing. To assess the colocalization of SEPT2 with Rab5- and Rab7-mCherry vesicles (Fig. S1), the analysis was restricted to non-tubular macropinosomes/endosomes in the peripheral lamellum, which was outlined as a 10-µm-wide zone from the cell edge. The fluorescence of non-tubular Rab5 and Rab7 macropinosomes/endosomes was masked, and submasks were made based on their overlap with SEPT2 fluorescence. The same approach was used to derive the percentage of ML1N-2x-GFP macropinosomes/endosomes, vesicles 0.5–5 μm^3 in size, with SEPT2. Presence of transferrin-488 in Rab11A-positive endosomes was quantified by using fluorescence intensity segmentations to mask Rab11A endosomes and Tf-488 particles 0.05–0.5 μm^3 in size. Tf-488 and Rab11A masks were subtracted to create a new artificial channel with masks that corresponded to all Tf-488 fluorescence that overlapped with Rab11A. The Rab11A-positive Tf-488 particles were counted, and their number was divided by the total number of Tf-488 particles. In Fig. 3 (B–D), time-lapse movies of PM-mCherry of identical capture intervals (5 s) and duration (8 min) were analyzed after applying the 2D Laplacian of Gaussian function, which improves the clarity of membrane vacuoles and tubules. The formation of nascent macropinosomes from membrane vesicles was tracked manually, and clusters of three or more macropinosomes per cell were scored (Fig. 3 B). Macropinosome lifetime was quantified by measuring the time that it took for a nascent macropinosome to disappear or merge with another membrane vacuole or tubule (Fig. 3 C). The number of nascent macropinosomes that fused with another membrane compartment was calculated as percentage of total macropinosomes tracked. The number of fusion events per minute was the inverse of the time that it took for a nascent macropinosome to undergo a fusion event (Fig. 3 D). In Fig. 3 E, 2-µm-long line masks were drawn along the membrane contact of two macropinocytic vacuoles and along their noncontacting perimeters. The intensity profiles of each line scan were exported and plotted in Excel. In Fig. 3 (F and G) and Fig. S2 (B and D), the number and size of dextran particles were quantified in ImageJ (National Institutes of Health) by generating masks of dextran fluorescence intensity, which were gated by size (0.2–20 μm^2) in confocal maximum-intensity projection images as previously done by others (Wang et al., 2014). The rates of lysosomal delivery of dextran corresponded to the slopes of the lines derived from a least squares linear regression fit to the 5-, 10-, and 30-min points of the plot in Fig. 4 C. In Fig. 5 (A and B), segmentation of fluorescence intensity was used to create TR-dextran, FITC-dextran, and LAMP1 masks. TR-dextran and LAMP1 masks were subtracted to create a new artificial channel with masks corresponding to LAMP1-positive TR-dextran particles. These masks were subsequently subtracted from FITC-dextran masks to identify the FITC-dextran particles that colocalize with LAMP1-positive TR-dextran. These particles were divided by the total number of FITC-dextran particles. In vitro fusion (Fig. 5) was quantified by generating fluorescence segmentation masks that correspond to FITC- and TR-dextran–containing macropinosomes/endosomes. The masks were subsequently subtracted from each other to identify macropinosomes/endosomes with overlapping fluorescence. The number of these new masks was automatically calculated and divided by the total number of macropinosomes/endosomes, which was calculated by subtracting the number of masks with FITC/TR overlap from the total number of FITC- and TR-labeled masks.

Statistical analyses

All datasets were analyzed using Shapiro and Levene tests, respectively, for normality and equal variance in R software, and unpaired Student's *t* test was used to derive p-values (95% confidence intervals) in Excel. All values represent the mean ± SEM.

Online supplemental material

Fig. S1 shows PM-mCherry and SEPT2 localization with respect to Rab5 and Rab7. Fig. S2 shows that SEPT2 depletion increases the size and number of macropinosomes in MDCK and HT1080 cells but does not affect the traffic of dextran to Rab5- and Rab7-positive macropinosomes/endosomes. Fig. S3 shows that SEPT2 does not affect endocytosis of transferrin or Vps39-GFP localization to macropinosomes/endosomes and does not colocalize with the exocyst subunits Sec6, Sec8, and Exo70 at sites of macropinosome contact. Video 1 shows the accumulation of SEPT2-GFP at the contact and fusion site of two macropinosomes. Video 2 shows that SEPT2 knockdown impairs macropinosome fusion and turnover. Video 3 shows that SEPT2 depletion does not inhibit the formation of membrane tubules from macropinosomes. Online supplemental material is available at http://www.jcb.org/cgi/content/full/jcb.201603030/DC1.

Acknowledgments

We thank Drs. James Nelson, Charles Yeaman, Victor Faundez, and Haoxing Xufor reagents. All microscopy was performed at Drexel University's Cell Imaging Center.

This work was supported by National Institutes of Health grants CA176910 (L. Dolat) and GM097664 (E.T. Spiliotis).

The authors declare no competing financial interests.

Submitted: 8 March 2016
Accepted: 21 July 2016

References

Bai, X., J.R. Bowen, T.K. Knox, K. Zhou, M. Pendziwiat, G. Kuhlenbäumer, C.V. Sindelar, and E.T. Spiliotis. 2013. Novel septin 9 repeat motifs altered in neuralgic amyotrophy bind and bundle microtubules. *J. Cell Biol.* 203:895–905. http://dx.doi.org/10.1083/jcb.201308068

Balderhaar, H.J., and C. Ungermann. 2013. CORVET and HOPS tethering complexes—coordinators of endosome and lysosome fusion. *J. Cell Sci.* 126:1307–1316. http://dx.doi.org/10.1242/jcs.107805

Barysch, S.V., R. Jahn, and S.O. Rizzoli. 2010. A fluorescence-based in vitro assay for investigating early endosome dynamics. *Nat. Protoc.* 5:1127–1137. http://dx.doi.org/10.1038/nprot.2010.84

Baumann, S., J. König, J. Koepke, and M. Feldbrügge. 2014. Endosomal transport of septin mRNA and protein indicates local translation on

endosomes and is required for correct septin filamentation. *EMBO Rep.* 15:94–102. http://dx.doi.org/10.1002/embr.201338037

Baust, T., M. Anitei, C. Czupalla, I. Parshyna, L. Bourel, C. Thiele, E. Krause, and B. Hoflack. 2008. Protein networks supporting AP-3 function in targeting lysosomal membrane proteins. *Mol. Biol. Cell.* 19:1942–1951. http://dx.doi.org/10.1091/mbc.E08-02-0110

Beites, C.L., H. Xie, R. Bowser, and W.S. Trimble. 1999. The septin CDCrel-1 binds syntaxin and inhibits exocytosis. *Nat. Neurosci.* 2:434–439. http://dx.doi.org/10.1038/8100

Benjamin, J.M., A.V. Kwiatkowski, C. Yang, F. Korobova, S. Pokutta, T. Svitkina, W.I. Weis, and W.J. Nelson. 2010. AlphaE-catenin regulates actin dynamics independently of cadherin-mediated cell-cell adhesion. *J. Cell Biol.* 189:339–352. http://dx.doi.org/10.1083/jcb.200910041

Bowen, J.R., D. Hwang, X. Bai, D. Roy, and E.T. Spiliotis. 2011. Septin GTPases spatially guide microtubule organization and plus end dynamics in polarizing epithelia. *J. Cell Biol.* 194:187–197. http://dx.doi.org/10.1083/jcb.201102076

Bridges, A.A., and A.S. Gladfelter. 2015. Septin form and function at the cell cortex. *J. Biol. Chem.* 290:17173–17180. http://dx.doi.org/10.1074/jbc.R114.634444

Bridges, A.A., M.S. Jentzsch, P.W. Oakes, P. Occhipinti, and A.S. Gladfelter. 2016. Micron-scale plasma membrane curvature is recognized by the septin cytoskeleton. *J. Cell Biol.* 213:23–32. http://dx.doi.org/10.1083/jcb.201512029

Bright, N.A., M.J. Gratian, and J.P. Luzio. 2005. Endocytic delivery to lysosomes mediated by concurrent fusion and kissing events in living cells. *Curr. Biol.* 15:360–365. http://dx.doi.org/10.1016/j.cub.2005.01.049

Bryant, D.M., M.C. Kerr, L.A. Hammond, S.R. Joseph, K.E. Mostov, R.D. Teasdale, and J.L. Stow. 2007. EGF induces macropinocytosis and SNX1-modulated recycling of E-cadherin. *J. Cell Sci.* 120:1818–1828. http://dx.doi.org/10.1242/jcs.000653

Caudron, F., and Y. Barral. 2009. Septins and the lateral compartmentalization of eukaryotic membranes. *Dev. Cell.* 16:493–506. http://dx.doi.org/10.1016/j.devcel.2009.04.003

Commisso, C., S.M. Davidson, R.G. Soydaner-Azeloglu, S.J. Parker, J.J. Kamphorst, S. Hackett, E. Grabocka, M. Nofal, J.A. Drebin, C.B. Thompson, et al. 2013. Macropinocytosis of protein is an amino acid supply route in Ras-transformed cells. *Nature.* 497:633–637. http://dx.doi.org/10.1038/nature12138

Connolly, D., I. Abdesselam, P. Verdier-Pinard, and C. Montagna. 2011. Septin roles in tumorigenesis. *Biol. Chem.* 392:725–738. http://dx.doi.org/10.1515/BC.2011.073

Corbett-Nelson, E.F., D. Mason, J.G. Marshall, Y. Collette, and S. Grinstein. 2006. Signaling-dependent immobilization of acylated proteins in the inner monolayer of the plasma membrane. *J. Cell Biol.* 174:255–265. http://dx.doi.org/10.1083/jcb.200605044

Davis, P.J., B.S. Handwerger, and F. Glaser. 1974. Physical properties of a dog liver and kidney cytosol protein that binds thyroid hormone. *J. Biol. Chem.* 249:6208–6217.

de Carvalho, T.M., E.S. Barrias, and W. de Souza. 2015. Macropinocytosis: A pathway to protozoan infection. *Front. Physiol.* 6:106. http://dx.doi.org/10.3389/fphys.2015.00106

Dolat, L., Q. Hu, and E.T. Spiliotis. 2014a. Septin functions in organ system physiology and pathology. *Biol. Chem.* 395:123–141. http://dx.doi.org/10.1515/hsz-2013-0233

Dolat, L., J.L. Hunyara, J.R. Bowen, E.P. Karasmanis, M. Elgawly, V.E. Galkin, and E.T. Spiliotis. 2014b. Septins promote stress fiber-mediated maturation of focal adhesions and renal epithelial motility. *J. Cell Biol.* 207:225–235. http://dx.doi.org/10.1083/jcb.201405050

Feliciano, W.D., S. Yoshida, S.W. Straight, and J.A. Swanson. 2011. Coordination of the Rab5 cycle on macropinosomes. *Traffic.* 12:1911–1922. http://dx.doi.org/10.1111/j.1600-0854.2011.01280.x

Fung, K.Y., L. Dai, and W.S. Trimble. 2014. Cell and molecular biology of septins. *Int. Rev. Cell Mol. Biol.* 310:289–339. http://dx.doi.org/10.1016/B978-0-12-800180-6.00007-4

Gu, Z., E.H. Noss, V.W. Hsu, and M.B. Brenner. 2011. Integrins traffic rapidly via circular dorsal ruffles and macropinocytosis during stimulated cell migration. *J. Cell Biol.* 193:61–70. http://dx.doi.org/10.1083/jcb.201007003

Hsu, S.C., C.D. Hazuka, R. Roth, D.L. Foletti, J. Heuser, and R.H. Scheller. 1998. Subunit composition, protein interactions, and structures of the mammalian brain sec6/8 complex and septin filaments. *Neuron.* 20:1111–1122. http://dx.doi.org/10.1016/S0896-6273(00)80493-6

Ito, H., K. Atsuzawa, R. Morishita, N. Usuda, K. Sudo, I. Iwamoto, K. Mizutani, R. Katoh-Semba, Y. Nozawa, T. Asano, and K. Nagata. 2009. Sept8 controls the binding of vesicle-associated membrane protein 2 to synaptophysin. *J. Neurochem.* 108:867–880. http://dx.doi.org/10.1111/j.1471-4159.2008.05849.x

Jefferies, H.B., F.T. Cooke, P. Jat, C. Boucheron, T. Koizumi, M. Hayakawa, H. Kaizawa, T. Ohishi, P. Workman, M.D. Waterfield, and P.J. Parker. 2008. A selective PIKfyve inhibitor blocks PtdIns(3,5)P(2) production and disrupts endomembrane transport and retroviral budding. *EMBO Rep.* 9:164–170. http://dx.doi.org/10.1038/sj.embor.7401155

Kerr, M.C., and R.D. Teasdale. 2009. Defining macropinocytosis. *Traffic.* 10:364–371. http://dx.doi.org/10.1111/j.1600-0854.2009.00878.x

Kerr, M.C., M.R. Lindsay, R. Luetterforst, N. Hamilton, F. Simpson, R.G. Parton, P.A. Gleeson, and R.D. Teasdale. 2006. Visualisation of macropinosome maturation by the recruitment of sorting nexins. *J. Cell Sci.* 119:3967–3980. http://dx.doi.org/10.1242/jcs.03167

Kerr, M.C., J.T. Wang, N.A. Castro, N.A. Hamilton, L. Town, D.L. Brown, F.A. Meunier, N.F. Brown, J.L. Stow, and R.D. Teasdale. 2010. Inhibition of the PtdIns(5) kinase PIKfyve disrupts intracellular replication of *Salmonella*. *EMBO J.* 29:1331–1347. http://dx.doi.org/10.1038/emboj.2010.28

Kimmelman, A.C. 2015. Metabolic dependencies in RAS-driven cancers. *Clin. Cancer Res.* 21:1828–1834. http://dx.doi.org/10.1158/1078-0432.CCR-14-2425

Levin, R., S. Grinstein, and D. Schlam. 2015. Phosphoinositides in phagocytosis and macropinocytosis. *Biochim. Biophys. Acta.* 1851:805–823. http://dx.doi.org/10.1016/j.bbalip.2014.09.005

Li, X., X. Wang, X. Zhang, M. Zhao, W.L. Tsang, Y. Zhang, R.G. Yau, L.S. Weisman, and H. Xu. 2013. Genetically encoded fluorescent probe to visualize intracellular phosphatidylinositol 3,5-bisphosphate localization and dynamics. *Proc. Natl. Acad. Sci. USA.* 110:21165–21170. http://dx.doi.org/10.1073/pnas.1311864110

Lim, J.P., and P.A. Gleeson. 2011. Macropinocytosis: An endocytic pathway for internalising large gulps. *Immunol. Cell Biol.* 89:836–843. http://dx.doi.org/10.1038/icb.2011.20

Martens, S., and H.T. McMahon. 2008. Mechanisms of membrane fusion: Disparate players and common principles. *Nat. Rev. Mol. Cell Biol.* 9:543–556. http://dx.doi.org/10.1038/nrm2417

McCartney, A.J., Y. Zhang, and L.S. Weisman. 2014. Phosphatidylinositol 3,5-bisphosphate: Low abundance, high significance. *BioEssays.* 36:52–64. http://dx.doi.org/10.1002/bies.201300012

Mercer, J., and A. Helenius. 2012. Gulping rather than sipping: Macropinocytosis as a way of virus entry. *Curr. Opin. Microbiol.* 15:490–499. http://dx.doi.org/10.1016/j.mib.2012.05.016

Mostowy, S., and P. Cossart. 2012. Septins: The fourth component of the cytoskeleton. *Nat. Rev. Mol. Cell Biol.* 13:183–194. http://dx.doi.org/10.1038/nrm3284

Oztan, A., M. Silvis, O.A. Weisz, N.A. Bradbury, S.C. Hsu, J.R. Goldenring, C. Yeaman, and G. Apodaca. 2007. Exocyst requirement for endocytic traffic directed toward the apical and basolateral poles of polarized MDCK cells. *Mol. Biol. Cell.* 18:3978–3992. http://dx.doi.org/10.1091/mbc.E07-02-0097

Pagano, A., P. Crottet, C. Prescianotto-Baschong, and M. Spiess. 2004. In vitro formation of recycling vesicles from endosomes requires adaptor protein-1/clathrin and is regulated by rab4 and the connector rabaptin-5. *Mol. Biol. Cell.* 15:4990–5000. http://dx.doi.org/10.1091/mbc.E04-04-0355

Paterson, H., B. Reeves, R. Brown, A. Hall, M. Furth, J. Bos, P. Jones, and C. Marshall. 1987. Activated N-ras controls the transformed phenotype of HT1080 human fibrosarcoma cells. *Cell.* 51:803–812. http://dx.doi.org/10.1016/0092-8674(87)90103-6

Poupon, V., A. Stewart, S.R. Gray, R.C. Piper, and J.P. Luzio. 2003. The role of mVps18p in clustering, fusion, and intracellular localization of late endocytic organelles. *Mol. Biol. Cell.* 14:4015–4027. http://dx.doi.org/10.1091/mbc.E03-01-0040

Racoosin, E.L., and J.A. Swanson. 1993. Macropinosome maturation and fusion with tubular lysosomes in macrophages. *J. Cell Biol.* 121:1011–1020. http://dx.doi.org/10.1083/jcb.121.5.1011

Schmees, C., R. Villaseñor, W. Zheng, H. Ma, M. Zerial, C.H. Heldin, and C. Hellberg. 2012. Macropinocytosis of the PDGF β-receptor promotes fibroblast transformation by H-RasG12V. *Mol. Biol. Cell.* 23:2571–2582. http://dx.doi.org/10.1091/mbc.E11-04-0317

Settembre, C., A. Fraldi, D.L. Medina, and A. Ballabio. 2013. Signals from the lysosome: A control centre for cellular clearance and energy metabolism. *Nat. Rev. Mol. Cell Biol.* 14:283–296. http://dx.doi.org/10.1038/nrm3565

Spiliotis, E.T., M. Kinoshita, and W.J. Nelson. 2005. A mitotic septin scaffold required for mammalian chromosome congression and segregation. *Science.* 307:1781–1785. http://dx.doi.org/10.1126/science.1106823

Swanson, J.A. 2008. Shaping cups into phagosomes and macropinosomes. *Nat. Rev. Mol. Cell Biol.* 9:639–649. http://dx.doi.org/10.1038/nrm2447

Tanaka-Takiguchi, Y., M. Kinoshita, and K. Takiguchi. 2009. Septin-mediated uniform bracing of phospholipid membranes. *Curr. Biol.* 19:140–145. http://dx.doi.org/10.1016/j.cub.2008.12.030

Taniguchi, M., M. Taoka, M. Itakura, A. Asada, T. Saito, M. Kinoshita, M. Takahashi, T. Isobe, and S. Hisanaga. 2007. Phosphorylation of adult type Sept5 (CDCrel-1) by cyclin-dependent kinase 5 inhibits interaction with syntaxin-1. *J. Biol. Chem.* 282:7869–7876. http://dx.doi.org/10.1074/jbc.M609457200

Traikov, S., C. Stange, T. Wassmer, P. Paul-Gilloteaux, J. Salamero, G. Raposo, and B. Hoflack. 2014. Septin6 and Septin7 GTP binding proteins regulate AP-3- and ESCRT-dependent multivesicular body biogenesis. *PLoS One.* 9:e109372. http://dx.doi.org/10.1371/journal.pone.0109372

Wang, J.T., R.D. Teasdale, and D. Liebl. 2014. Macropinosome quantitation assay. *MethodsX.* 1:36–41. http://dx.doi.org/10.1016/j.mex.2014.05.002

White, E. 2013. Exploiting the bad eating habits of Ras-driven cancers. *Genes Dev.* 27:2065–2071. http://dx.doi.org/10.1101/gad.228122.113

Yoshida, S., A.D. Hoppe, N. Araki, and J.A. Swanson. 2009. Sequential signaling in plasma-membrane domains during macropinosome formation in macrophages. *J. Cell Sci.* 122:3250–3261. http://dx.doi.org/10.1242/jcs.053207